Materials Chemistry and Physics 296 (2023) 127275

Contents lists available at ScienceDirect

Materials Chemistry and Physics

journal homepage: www.elsevier.com/locate/matchemphys

Photocatalytic enhancement mechanisms for novel g-C_3N_4/PVK nanoheterojunction

V.W. Elloh [a,b,*], E. Okoampa Boadu [b], D. Abbeyquaye [b], D.E. Anderson [b], A. Yaya [c]

[a] Department of Physics, University of Petroleum and Energy Studies (UPES), Dehradun, India
[b] Department of Biomedical Engineering, Koforidua Technical University, Koforidua, Ghana
[c] Department of Materials Science and Engineering, University of Ghana, Legon, Ghana

HIGHLIGHTS

- Band alignment ensures photogenerated electrons migrate from g-C_3N_4 to PVK monomer.
- High hydrogen-evolution reaction activity.
- Charge transfer between g-C_3N_4 monolayer and PVK results.
- Polarized field within interface region separation of photogenerated carriers.
- PVK is a non-noble metal co-catalyst for g-C_3N_4 photocatalysis.

ARTICLE INFO

Keywords:
DFT
GGA
PBE
LDA
Monolayer g-C_3N_4
PVK
Photocatalytic semiconductor

ABSTRACT

The interactions between monolayer graphitic carbon nitride (g-C_3N_4) and conjugated polymer poly(9-vinylcarbazole) (PVK) have been explored. We investigated the enhanced photocatalytic mechanisms for the novel g-C_3N_4/PVK nanoheterojunction covering the state-of-the-art of DFT by performing rigorous DFT calculations combined with van der Waals corrections (GGA + vdW). The calculated band alignment between g-C_3N_4 monolayer and PVK monomer clearly reveals that the conduction band minimum and the valence band maximum of g-C_3N_4 monolayer are higher than those of the conjugated polymer PVK. This predicted band alignment ensures the photogenerated electrons easily migrate from the g-C_3N_4 monolayer to the PVK monomer, and will lead to high hydrogen-evolution reaction activity. The charge transfer between g-C_3N_4 monolayer and PVK results in a polarized field within the interface region, which will benefit the separation of photogenerated carriers. The calculated density of electronic states, Lowdin charge transfer and charge density difference certify that this proposed layered nanoheterojunction is an excellent light-harvesting semiconductor. These findings indicate that the conjugated polymer PVK is a promising candidate as a non-noble metal co-catalyst for g-C_3N_4 photocatalysis. It also provides useful information for understanding the observed enhanced photocatalytic mechanisms in experiments.

1. Introduction

The world has witnessed a great deal of increase in environmental challenges and energy demands as a consequence of the depletion of fossil fuels for some number of decades now. By way of addressing the above challenges, various technologies have been proposed. One of them is semiconductor photocatalysis. This is a potential technology proposed to address the environmental problems. This technology involves converting the raw material CO_2 into chemical solar fuels [1–9]. Semiconductor photocatalysis is a novel and efficient technology. It has attracted tremendous attention of researchers and industrialists due to its versatile applications in solar energy utilization and pollutant elimination [3,10–12]. Semiconductor photocatalysts like TiO_2, ZnO and $SrTiO_3$ are known to exhibit high photocatalytic performance [13]. However, they can only use a few per cent of the solar energy because of their wide energy band gaps. Photocatalysts like CdS has suitable band gap to absorb visible light. Concurrently, photogenerated electrons of conduction bands have sufficient reducing ability for photocatalytic

* Corresponding author. Department of Physics, University of Petroleum and Energy Studies (UPES), Dehradun, India.
E-mail address: vanw.elloh@ktu.edu.gh (V.W. Elloh).

https://doi.org/10.1016/j.matchemphys.2022.127275
Received 6 September 2022; Received in revised form 10 December 2022; Accepted 24 December 2022
Available online 27 December 2022
0254-0584/

hydrogen evolution. However, CdS lacks stability because of the self-oxidation of photogenerated holes. For the surpassing reasons, it is prudent to search for novel high-efficient photocatalytic materials.

g-C_3N_4 was reported by Wang et al. [14] to be able to generate hydrogen from water under visible light. Two-dimensional layered g-C_3N_4 has the appropriate band gap. It has unique physicochemical properties such as high thermal and chemical stability, unique electronic properties, low density and extreme hardness [15–18]. These properties make g-C_3N_4 an excellent potential material for application in a wide range of areas such as photocatalytic CO_2 reduction, fuel cells, pollutant removal, photochemical water splitting for hydrogen production, environmental remediation [1,3,10,19–22]. Therefore, g-C_3N_4 is considered a promising candidate for visible-light photocatalytic hydrogen generation, organic pollutant decomposition and carbon dioxide reduction. However, g-C_3N_4 suffers from a high recombination rate of photogenerated electrons and holes. This leads to low quantum efficiency [23]. The possibility to restrain the high recombination rate of photogenerated electron−hole pairs is crucial to improve the poor quantum efficiency of g-C_3N_4.

Various modification techniques have been explored in recent times to optimize the performance of g-C_3N_4 [24–26]. Band-gap engineering, micro-nanostructuring, surface modifications, cocatalyst combination, semiconductor coupling, heterojunction formation are just but a few to mention. For example, band-gap engineering through metal and nonmetal elements doping has been studied. It inhibits photogenerated electron-hole pair recombination and greatly increases the light-harvesting ability in the visible region in pristine g-C_3N_4 [27–29]. In order to increase the surface area of g-C_3N_4, various modification strategies have been explored and observed to be effective [2,3,23, 30–34]. A study conducted by Zhu et al. based on DFT calculations shows that halogen-doped monolayer g-C_3N_4 systems tend to have narrow band-gaps and increase light absorption rate which are required for high photocatalytic activity [30].

Recently, construction of g-C_3N_4/semiconductor heterostructures demonstrated an enormous potential to promote the photocatalytic performance of g-C_3N_4 mediated by efficient separation of the electron−hole pairs, thereby restraining the recombination rate of photogenerated carriers [35–40]. g-C_3N_4/semiconductor heterojunctions have exhibited enhanced photocatalytic activity. In particular, the monolayer g-C_3N_4/semiconductor heterostructure exhibits significantly enhanced photocatalytic hydrogen production and dye degradation under visible-light irradiation [41,42]. The mechanisms of photocatalysis enhancements in g-C_3N_4/semiconductor nanoheterojunctions, however, remain unclear. The band structure, charge transfer and interface interactions of the g-C_3N_4/semiconductor nanoheterojunctions have not been fully investigated. To this end, we seek to understand the mechanisms of enhanced photocatalysis in the g-C_3N_4/PVK nanoheterojunction and to further design a novel g-C_3N_4-based nanoheterostructures for visible-light harvesting photocatalysis. In this paper, we perform DFT calculations combined with van der Waals corrections (GGA + vdW) to investigate the structural and electronic properties of pristine g-C_3N_4 and g-C_3N_4/PVK nanoheterojunction.

2. Computational methods

All calculations in this study are based on the methods of DFT and the ab-initio pseudo-potential plane wave basis set as implemented in the PWSCF code of the Quantum ESPRESSO [43]. We performed the calculation within the local density approximation (LDA), parameterized by Perdew and Zunger [44], the generalized gradient approximation (GGA) of Perdew, Burke and Ernzerhof (PBE) [45]. The Kohn-Sham orbitals are expanded in a plane-wave basis set. The electronic wave functions and the charge density are expanded in plane waves up to 30 Ry and 180Ry respectively. The core and valence electrons are treated with Vanderbilt ultrasoft pseudopotentials [46]. The g-C_3N_4/PVK nanoheterostructure was simulated using periodic boundary conditions and a supercell approximation with lattice parameters $a = 6.511$ Å, $b = 6.511$ Å and $c = 4.745$ Å. The sampling of the Brillouin zone was done using a $9 \times 9 \times 1$ grid and tested to give convergent results for the total energy. In this work, the Grimme's D3 correction term [47] is applied to include the van der Waals (vdW) interaction which is found to be substantial in carbon nano systems [48–50]. The vacuum layer in the simulation cell is set to 12 Å thick in both y- and z-directions to ensure negligible interactions between the supercell and its periodic images.

The structural optimizations were performed using a conjugated gradient procedure. For the nanoheterostructure, we have chosen the position and the orientation in which the whole system has minimum energy. For this position and orientation, the structure is fully relaxed until all the force components were smaller than 0.4×10^{-2} Ry bohr^{-1} (~ 0.1 eV Å^{-1}), in order to obtain the exact position and orientation for the nanoheterojunction.

3. Results and discussions

3.1. Geometry and structure of monolayer g-C_3N_4 and PVK unit cells

Fig. 1 is a schematic illustration of (a) monolayer g-C_3N_4 and (b) PVK monomer, *N*-vinylcarbazole structures. Graphitic carbon nitride, g-C_3N_4, is a metal-free, highly efficient, durable, low-cost and earth-abundant semiconductor [1]. g-C_3N_4 is a polymeric semiconductor with a band-gap of approximately 2.7 eV [3]. It is easily synthesized through thermal condensation of simple and cheap precursors like urea, cyanamide, dicyandiamide, melamine, etc. [10]. Also, it.

has unique physicochemical properties such as high thermal and chemical stability, unique electronic properties, low density and extreme hardness [12]. These properties make g-C_3N_4 an excellent potential material for application in a wide range of areas such as photocatalytic CO_2 reduction, fuel cells, pollutant removal, photochemical water splitting for hydrogen production, environmental remediation, etc. [13–15]. Nevertheless, serious limitations of pristine g-C_3N_4 are its poor visible light utilization ability, fast recombination of photogenerated electron-hole pairs, i.e., low mobility of charge carriers and low surface area [10–12,16]. Poly(9-vinylcarbazole) (PVK) is a conjugated polymer with hydrophobic properties. PVK films are mainly used as holes. (PVK) is a temperature-resistant [51] thermoplastic polymer produced by radical polymerization from the monomer, *N*-vinylcarbazole. It is photoconductive and thus the basis for photorefractive polymers and organic light-emitting diodes [52]. Poly (9-vinylcarbazole), a conjugated polymer has been explored as an efficient hole transport material for the preparation of p-i-n type, inverted planar heterojunction perovskite solar cells. Poly(N-vinyl carbazole) as a hole transport organic semiconducting polymer has been widely used as an electronic and optical material [53]. PVK is used to synthesize titanium oxide (TiO_2) quantum dots fillers that find potential applications as donor-acceptor layers in polymeric solar cells [54]. PVK is used to functionalize carbon nanotubes (CNTs) and form conductive reinforcements on epoxy groups [55]. Iridium composites are normally surface modified by PVK for the fabrication of highly efficient organic light emitting devices. The electrical conductivity of PVK changes according to intensity of illumination. As a consequence, PVK is classified as a semiconductor or photoconductor. Poly (9-vinylcarbazole) is extremely brittle, but its brittleness can be reduced by copolymerization with a small amount of isoprene [56].

3.2. Structural properties

The structural geometry and stability of PVK interacting with monolayer g-C_3N_4 as a nanoheterojunction model in a supercell structure was studied. We examined different structural geometries and stability of PVK polymer chain interacting with monolayer g-C_3N_4. The PVK polymer chain was aligned parallel to the monolayer g-C_3N_4 along

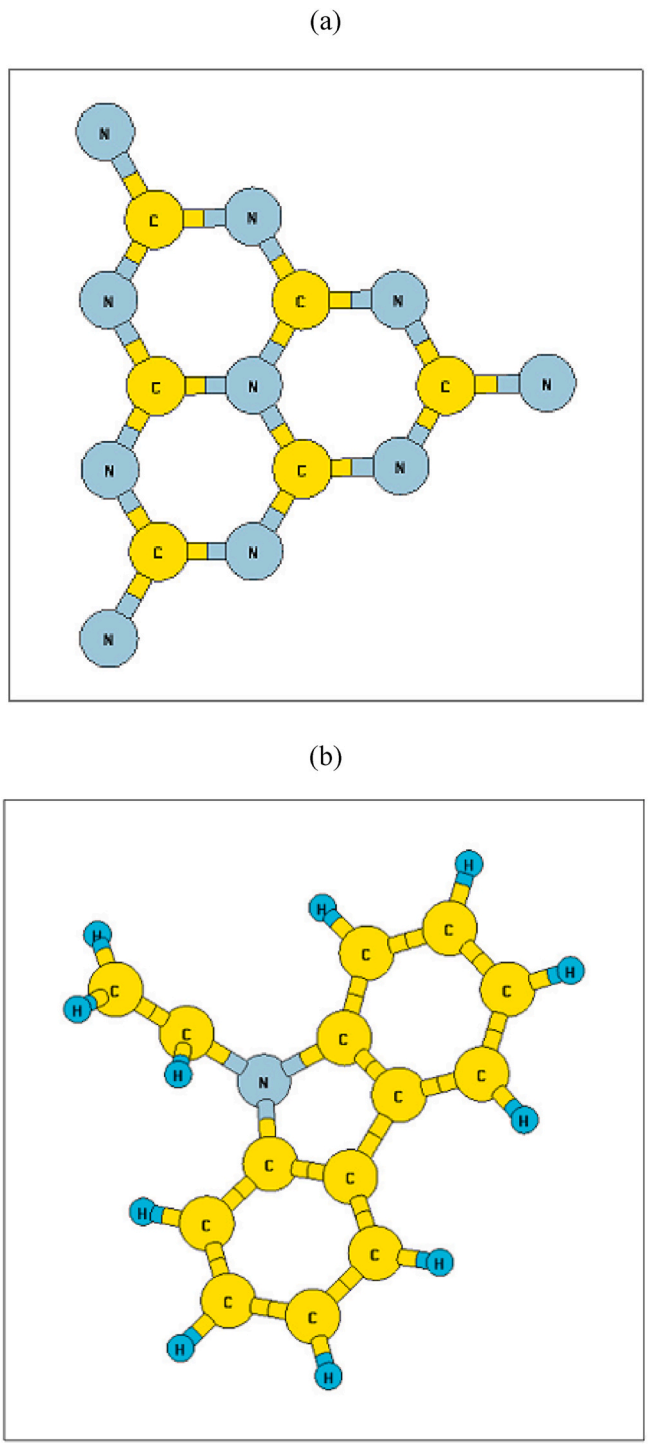

Fig. 1. Schematic illustrations of (a) monolayer g-C_3N_4 and (b) PVK monomer unit cell used in this work.

with its side groups towards and/or away from the monolayer g-C_3N_4. Other structural combinations and orientations notably with the PVK curved around the monolayer g-C_3N_4 and by flipping the PVK through 180° about its centre were considered in order to determine the preferred orientation of the g-C_3N_4/PVK geometry. It was found that the PVK polymer chain preferred to align with its side groups towards the g-C_3N_4. We noted that the enthalpy of formation for this particular structural arrangement was lower than that of all other orientations examined. This is therefore energetically more stable and favorable. This orientation was therefore used for this study. We noted that the enthalpy of formation for this composite g-C_3N_4/PVK is low compare to similar structures in literature, therefore, energetically stable. Additionally, the negative formation energy implies composite is thermodynamically favorable for studies. A separation distance of ~3.383 Å was kept between monolayer g-C_3N_4 and PVK monomer for all the different nanoheterojunction orientations examined. This interlayer distance is comparable to the interlayer separations in graphite (ca. 3.35 Å). We computed the structural stability of the nanoheterojunction, g-C_3N_4/PVK, studied by using equations (1) and (2). Relative to this adsorption distance of 3.383 Å, we calculated the adsorption energy, E_{ad}, for the g-C_3N_4/PVK nanoheterojunction as recorded in Table 2. The adsorption energy, E_{ad}, was determined from the relation [1] below [57].

$$E_{ad} = \left(E_{PVK/g-C_3N_4} - E_{PVK} - E_{g-C_3N_4}\right) \quad (1)$$

where $E_{PVK/g-C_3N_4}$, E_{PVK}, $E_{g-C_3N_4}$ represent the total ground-state energy of the g-C_3N_4/PVK composite, the total energy of PVK, the total energy of g-C_3N_4 respectively predicted by DFT calculation. Quantum Espresso code reports the value of dispersion contribution to total energy for every step during the geometry optimization process. Accordingly, the dispersion contribution to adsorption energy was determined using Equation (1) above, by replacing the terms on the right-hand side with the dispersion contribution quantities for the converged geometry of each structure.

Whenever the $E_{ad} > 0$, then it suggests that the surface adsorption is thermodynamically feasible. The greater the E_{ad} value, the tendency of the adsorbate molecule to bind on the g-C_3N_4/PVK nanoheterostructure surface becomes stronger. From Table 2, a clear distinctive tendency of the monolayer g-C_3N_4 to adsorb favorably on PVK monomer surface is seen.

From DFT optimized configuration of the system considered, we calculated $E_{ad} \sim 2.236$ eV for GGA + vdW exchange-correlation functional and $E_{ad} \sim$ 2.129 eV for LDA exchange-correlation functional. The adsorption energies, $E_{ad} \sim 2.236, 2.129$ eV, for the respective exchange-correlation functionals, are attributed to the orientation and proximity of the nitride functional group of the conjugated polymer and to the π-electrons of the g-C_3N_4 and also via strong π-π interactions between the carbazole unit and the g-C_3N_4 to chemisorb at the g-C_3N_4/PVK surface.

For detail insight into the new structure, we calculated the formation energy per atom, E_{pa}, for monolayer g-C_3N_4 and the formation energy per atom for PVK separately and found their values to be −6.486 eV and −5.263 eV respectively. The formation energies were determined from the relation:

$$\Delta E = E_{CHN} - N_C E_C - N_H E_H - N_N E_N \quad (2)$$

where E_{CHN} is the total energy of the ground state of the corresponding nanoheterojunction modelled. E_C is the total energy of carbon in its ground state (graphite), N_C is the number of carbon atoms in the nanoheterojunction. E_H is the total energy of ground state of H, N_H is the number of hydrogen atoms in the nanoheterojunction, E_N is the total energy of ground state of N and N_N is the number of nitrogen atoms in the nanoheterojunction modelled. The calculated formation energies per atom for each of the systems considered is tabulated in Table 2. It is observed that the new nanoheterojunction modelled has large negative formation energy value per atom; an indication that this new structure is thermodynamically stable. It can be seen that the formation energy per atom values for g-C_3N_4 and PVK individually are much larger than the formation energy per atom value for g-C_3N_4/PVK as depicted in Table 2. This shows that the new nanoheterojunction is more stable and thermodynamically favorable compare to the original molecules. Furthermore, our calculations reveal that the new nanoheterojunction modelled is stable in both GGA + vdW and LDA model types. The value of the energy difference E_0(eV) for the simulated nanoheterojunction exhibits structural stability over g-C_3N_4 and PVK as shown in Table 1. The calculated band gap values along with the optimized lattice parameters

Table 1
Optimized Lattice Parameters a(Å), b(Å), c(Å), Energy gap Eg(eV) and Energy Difference E_0(eV) of PVK, g-C_3N_4 and g-C_3N_4/PVK nano structures.

	a(Å)	b(Å)	c(Å)	Eg(eV)	E_0(eV)
PVK	4.451	4.451	2.423	3.751	7.660
g-C_3N_4	4.277	4.505	2.293	2.692	6.021
g-C_3N_4/PVK	6.511	6.511	4.745	2.143	0.00

Table 2
Adsorption energy, E_{ad}, and formation energy per atom, E_{pa}, calculated using Equations (1) and (2).

(GGA + vdW)	$\mathbf{E_{ad}}/eV$	$\mathbf{E_{pa}}/eV$
PVK		−5.263
g-C_3N_4		−6.486
g-C_3N_4/PVK	2.236	−9.021
(LDA)		
PVK		−4.327
g-C_3N_4		−5.746
g-C_3N_4/PVK	2.129	−8.331

and other structural values of all the systems are presented in Table 1. The calculated bond lengths of C–N are 1.33 and 1.46 Å, which is in agreement with experimental bond length of C–N 1.32 and 1.44 Å.

The negative formation energy indicates that this heterostructure is energetically favorable and could be easily obtained. Furthermore, the binding energy, E_b, between g-C_3N_4 monolayer and PVK monomer in the nanoheterojunction is calculated to be ~ 21.14 meV/Å^2 which is close to the typical van der Waals binding energy, E_b, of ~ 20 meV/Å^2 by other advanced DFT calculations [58]. Hence, the g-C_3N_4/PVK nanoheterojunction belongs to van der Waals (vdW) heterostructures.

3.3. Electronic properties

The calculated band structures for PVK monomer, monolayer g-C_3N_4 and g-C_3N_4/PVK nanoheterojunction are respectively illustrated in Fig. 2(a, b & c). For the PVK monomer, the minimum energy gap of about 3.751 eV is an indirect bandgap transition from the top of the valence band maximum (VBM) located at the Γ point and the bottom of the conduction band minimum (CBM) located at the midpoint in-between the X and the Γ high symmetry points of the Brillouin zone. In the case of the monolayer g-C_3N_4, with a minimum energy gap of about 2.692 eV, an indirect bandgap transition from the top of the valence band maximum (VBM) is located at the Γ point and the bottom of the conduction band minimum (CBM) is located at the midpoint in-between the K and the X high symmetry points. The g-C_3N_4/PVK nanoheterojunction has a direct energy gap of approximately 2.143 eV, with both CBM and VBM located at the Γ-point as seen in Fig. 2(c). The Γ-to-Γ direct band gap guarantees the high efficiency energy conversion by solar energy without any lattice dynamic behaviour.

The band gap value 2.143 eV satisfies the required minimum band gap, $E_g > 1.23$ eV, showing the potential application of g-C_3N_4/PVK vdW nanoheterostructure for photocatalytic processes. Furthermore, the band edge alignments with respect to water reduction and oxidation potential levels of the g-C_3N_4/PVK nanoheterojunction satisfy photocatalytic water splitting. As is seen, PVK monomer has a favorable band position for water splitting, which is in accordance with other works [59,60]. For g-C_3N_4/PVK vdW nanoheterostructure, the VBM locates more positive than the water oxidation potential and the CBM is more negative than the hydrogen reduction potential, the feature of which is necessary for water splitting. The realignment of both VBM and CBM of the g-C_3N_4/PVK nanoheterostructure is attributed to the weak vdW interactions between monolayer g-C_3N_4 and PVK monomer. Further, since the VBM position with respect to water oxidation potential is much more

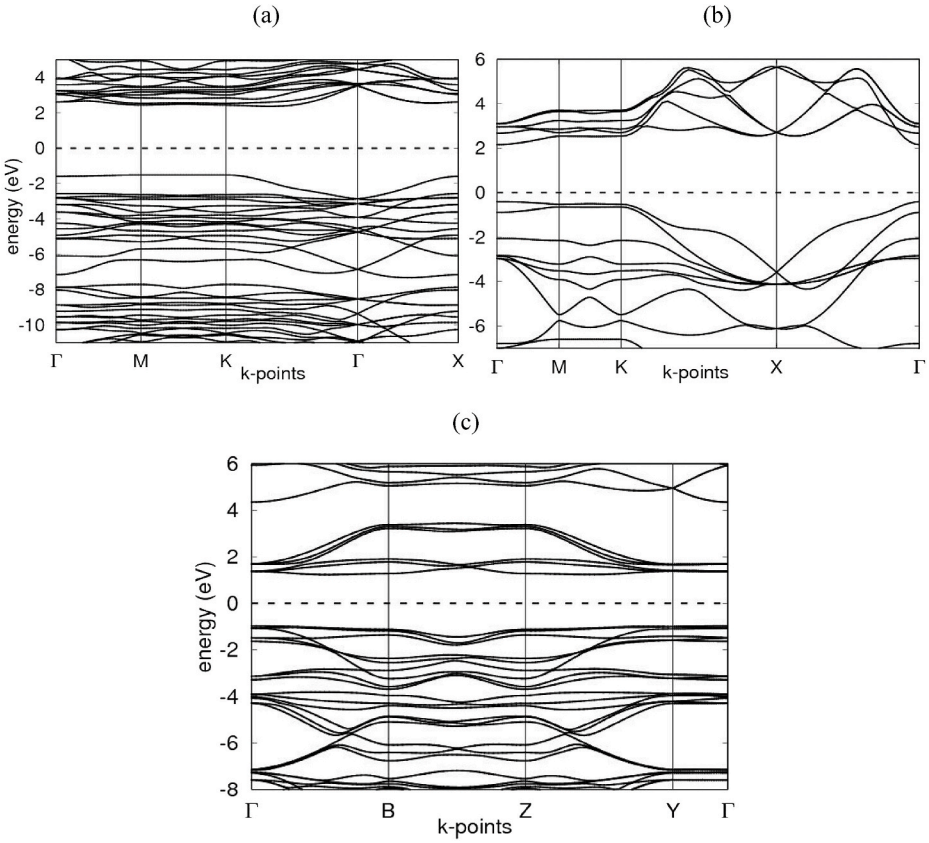

Fig. 2. Calculated band structures at high-symmetry k-points for (a) PVK, (b) monolayer g-C_3N_4 and (c) g-C_3N_4/PVK nanoheterojunction respectively. The Fermi energy level, E_F, is fixed as the reference of zero energy.

positive for g-C_3N_4/PVK, it indicates that better photocatalytic performance will be expected in g-C_3N_4/PVK vdW nanoheterostructure.

3.3.1. Analysis of the electronic density of states

Analysis of the nature of interactions and origin of energy gaps in the new nanoheterojunction is carried out by way of plotting the projected electronic density of states (DOS), partial electronic density of states (p-DOS), projected electronic density of states (DOS)-total electronic density of states (t-DOS) superimposed and total electronic density of states (t-DOS) for PVK, g-C_3N_4 and g-C_3N_4/PVK nanoheterojunction in Figs. 3–6 respectively. For the sake of comparison, the Fermi energy level, E_F, was set as zero on the energy scale of the energy band-gaps, Eg, between the occupied atomic orbitals and the empty atomic bands and the same for the DOS, which are shown in Figures (3-6). For PVK: the projected electronic density of states (DOS) plot, Fig. 3(a), shows that the entire portion of the DOS between −4 eV and 4 eV is due to H. The partial electron density of states (p-DOS) plot, Fig. 4(a), the occupied states are due largely to p-states of N and the bottom of the conduction band minimum are entirely p-states of C.

For monolayer g-C_3N_4: the projected electronic density of states (DOS) plot, Fig. 3(b), the portion of DOS below -1eV is due to N atoms and the portion which is above 1eV is also due to the contributions from N atoms. The partial electron density of states (p-DOS) plot, Fig. 4(b), the occupied states are due largely to p-states of N and the bottom of the conduction band minimum are entirely p-states of N.

For the g-C_3N_4/PVK nanoheterojunction: the projected electronic density of states (DOS) plot, Fig. 3(c), the portion of DOS below -1eV is due to N atoms and in similar manner, the portion which is above 1eV is due to contributions from C atoms. The partial electron density of states (p-DOS) plot, Fig. 4(c), the occupied states are due mainly to p-states of N and the bottom of the conduction band minimum are entirely s-states of N.

3.3.2. Photocatalytic properties analysis

Further analysis of the band state characterizations demonstrates that CBM and VBM are localized in different monolayers of the g-C_3N_4/PVK vdW heterostructures. The CBM originates from the N-s states in the PVK monomer, while the VBM is occupied by the N-p states in the g-C_3N_4 monolayer. In order to understand the role of the constituent layers in photocatalytic water splitting for g-C_3N_4/PVK vdW heterostructure, the band-decomposed charge density was calculated for the lowest unoccupied molecular orbital (LUMO, CBM at the Γ point) and the highest occupied molecular orbital (HOMO, VBM at the Γ point). As seen from the partial density of states (p-DOS) in Fig. 4(c), the LUMO is mainly contributed by the N-s orbitals, and the HOMO mainly consists of the N-p orbitals for the g-C_3N_4/PVK vdW heterostructures. The nature of the band states implies that the photoexcited electrons will transfer from the states localized in g-C_3N_4 to the states localized in PVK during the photocatalysis process, where PVK behaves as the electron acceptor and g-C_3N_4 behaves as the electron donor.

Consequently, during the photocatalytic water splitting the hydrogen production process takes place in the PVK monomer, while the oxygen production locates at the g-C_3N_4 monolayer. On the basis of the above analysis, the mechanism of the solar energy driven g-C_3N_4/PVK vdW heterostructure for the water splitting process is illustrated in Ref. [61]. When the incoming solar light is absorbed by the g-C_3N_4/PVK

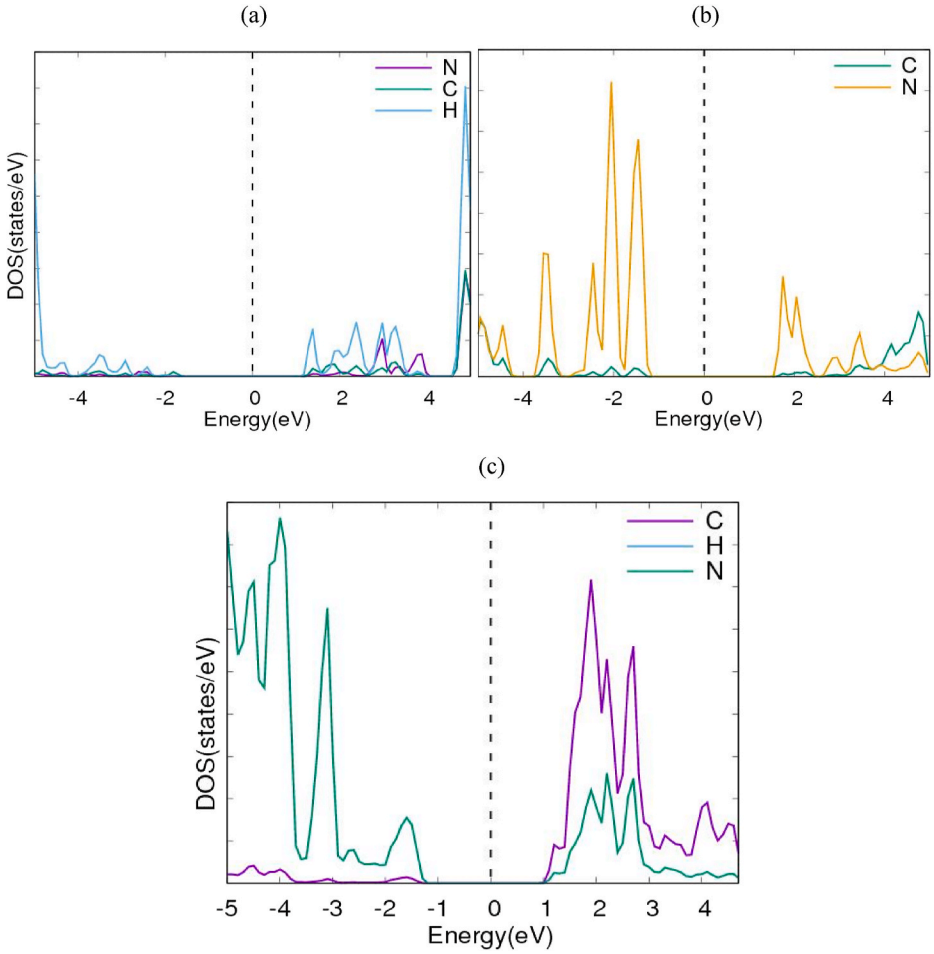

Fig. 3. Projected electronic density of states (DOS) for (a) PVK, (b) monolayer g-C_3N_4 and (c) g-C_3N_4/PVK nanoheterojunction respectively. The Fermi energy level, E_F, is set as zero on the energy scales.

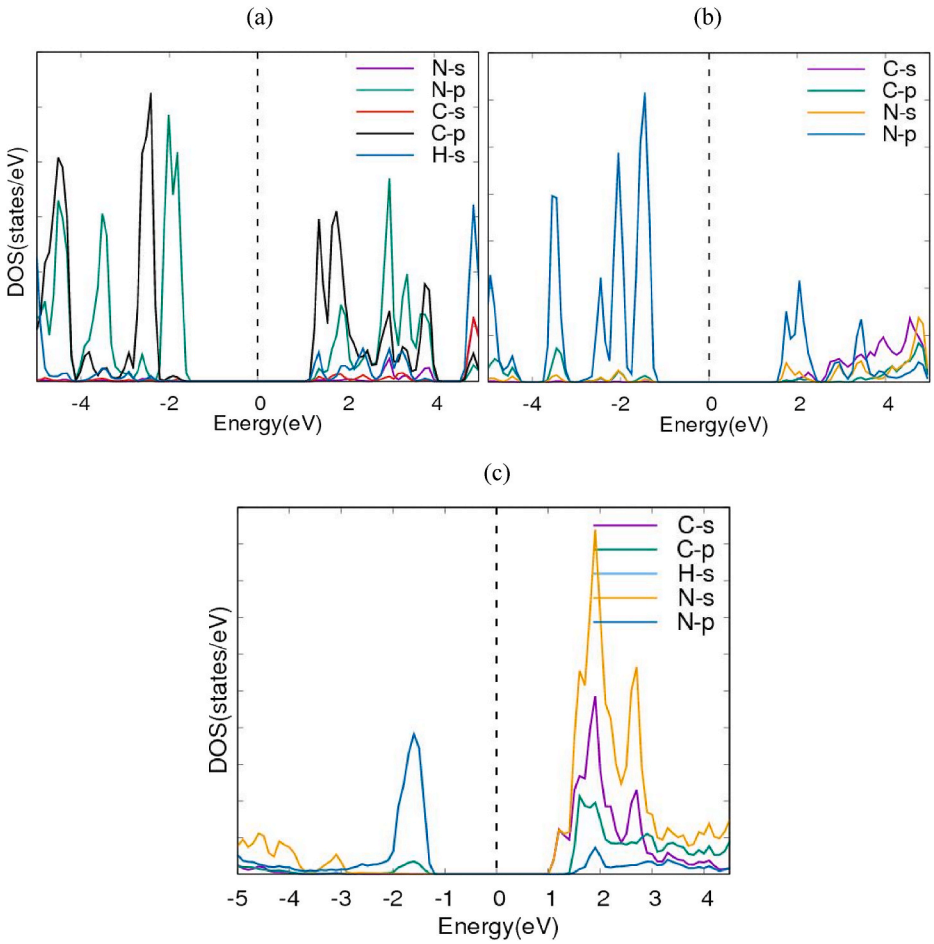

Fig. 4. Partial density of states (p-DOS) for (a) PVK, (b) monolayer g-C_3N_4 and (c) g-C_3N_4/PVK nanoheterojunction respectively. The Fermi energy level, E_F, is fixed as the reference of zero energy.

vdW heterostructure, photogenerated electrons will transfer from VBM to CBM, and hence hydrogen and oxygen will be separately produced at the PVK monomer and the g-C_3N_4 monolayer during the photocatalytic water splitting. This is because the vdW heterostructure shows direct and suitable band gap at the Γ point. The orbital overlap modifies the orbital and enhances the optical absorption. We have illustrated the density of states (DOS) of the g-C_3N_4/PVK vdW heterostructures in Fig. 3 (c) to further understand the optical absorption mechanism of the nanoheterojunction. The partial DOS in Fig. 4(c) shows the overlap of N-s and N-p electrons in the valence bands of the g-C_3N_4/PVK vdW nanoheterojunction. On the other hand, the g-C_3N_4/PVK vdW nanoheterojunction exhibits the requisite absorption spectra in the visible-light range, and thus the photocatalysis performance of the g-C_3N_4/PVK vdW nanoheterojunction is expected to be optimal. Nevertheless, the advantage of g-C_3N_4/PVK vdW nanoheterojunction over monolayer g-C_3N_4 is clear. The vdW nanoheterojunction not only has significantly improved photocatalysis properties but also can separately produce hydrogen and oxygen at the opposite monolayers of the vdW heterostructures. This is the mostly desired photocatalysis performance in practice, which however has been achieved in the current work.

3.3.3. Lowdin charge transfer

The amount of charge transfer from g-C_3N_4 to the PVK was estimated by projecting the charge density onto the atomic orbitals. We calculated the charge transfer as the difference between the Lowdin charges for pristine PVK and g-C_3N_4/PVK with the adsorbate molecules. From this result, we determined whether the adsorbate molecule acts as an acceptor or as a donor. The charge transfer from the monolayer g-C_3N_4 to the polymer PVK monomer in the g-C_3N_4/PVK nanoheterojunction turns out to be 0.39 electrons. Here we would like to point out that it is important to note that the size of the charge transfer slightly depends on the method chosen for calculations.

3.3.4. Charge density

The surface distribution of the electronic charge density gives the variation in the electronic density induced by the internal charges. Fig. 7 shows for g-C_3N_4/PVK nanoheterojunction the electronic charge densities distribution in response to internal electric field obtained by using Xcrysden software, version 1.5.60 [62]. The contributions to the charge density from different atoms are clearly visible from Fig. 7. It is apparent that the polarization of the surface charges is dependent on the atomic environment. Notable differences can be found in the surface charge distribution densities for the pristine aromatic polymers such as the benzene rings and for the carbon atoms and the π-conjugate plane of PVK, especially in the vicinity of the heteroatom nitrogen. Furthermore, from the figure, the polarizabilities are strongly anisotropic with a relatively large response for the surface charge distributions towards the π-conjugate plane of PVK.

The charge density plot in Fig. 7 shows a homogenous charge distribution among the nitrogen, hydrogen and carbon atoms signifying that a significant interaction took place. In terms of charge distribution, there is a uniform sharing between the nitrogen and carbon atoms with respective to electronegativity values of 3.04 and 2.55. There is also an excellent charge distribution between the hydrogen and carbon atoms because of similar electronegativity values of 2.20 and 2.55 respectively.

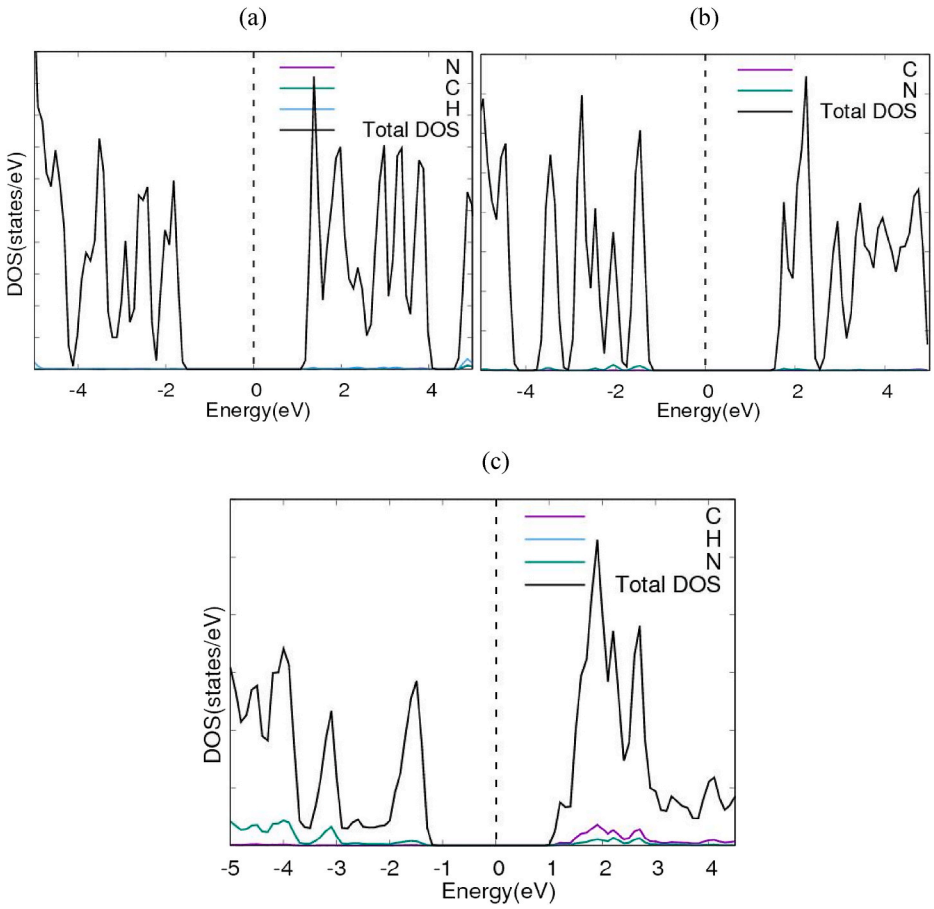

Fig. 5. Projected electronic density of states (DOS) and total DOS (t-DOS) superimposed for (a) PVK, (b) monolayer g-C_3N_4 and (c) g-C_3N_4/PVK nanoheterojunction respectively. The Fermi energy level, E_F, is set as zero on the energy scales.

The PDOS in Fig. 4 indicates that the p-orbitals of carbon and nitrogen atoms contributed most significantly to the total density of states. The reason for this can be traced back to the charge density plot in Fig. 7. The plot shows a higher density of charges around the carbon and nitrogen atoms. This is apparently due to nitrogen having comparable electronegativity value to that of carbon. As a result, the carbon and nitrogen atoms draw more electrons to themselves.

3.3.5. *Optical properties*

3.3.5.1. Calculated ultra violet optical absorption. Fig. 8(a, b & c) show calculated optical spectral absorption for pristine PVK, pristine monolayer g-C_3N_4 and g-C_3N_4/PVK nanoheterojunction respectively. Fig. 8(a) shows the absorption spectra for PVK without the monolayer g-C_3N_4. Fig. 8(b) shows the absorption spectra for the monolayer g-C_3N_4 without PVK. Fig. 8(c) is the calculated absorption spectra for the nanoheterojunction when the monolayer g-C_3N_4 was added to PVK. In Fig. 8 (a), it can be observed that there are five intensity peaks located at 0.41, 0.45, 0.49, 0.51 and 0.53 Ry. The most intense peak is located at 0.41 Ry. In Fig. 8(b), we observed that there are three intensity peaks located at 0.41, 0.45 and 0.67 Ry with the most intense peak located at 0.67 Ry. Comparing Fig. 8(c), it is observed that the addition of monolayer g-C_3N_4 to PVK has resulted in the quenching of the intensity peaks located at the various energies in the pristine monolayer g-C_3N_4 and PVK optical absorption spectra. This observation is an indication of charge transfer processes occurring between the monolayer g-C_3N_4 and PVK.

4. Conclusions

We have performed detailed DFT calculations to explore the enhanced photocatalytic mechanism for the novel hybrid g-C_3N_4/PVK nanoheterojunction. The calculated band alignment between the g-C_3N_4 monolayer and the PVK monomer reveals that the CBM (VBM) of g-C_3N_4 is higher than that of the CBM (VBM) of the PVK monomer. This predicted band alignment ensures the photogenerated electrons can easily migrate from the g-C_3N_4 layer to the PVK monomer, and leads to high hydrogen-evolution reaction activity. The charge transfer between PVK and g-C_3N_4 results in a polarized field within the interface region, which can effectively improve the separation efficiency of these photogenerated carriers. In addition, this new hybrid layered junction has high-light absorption ability. The g-C_3N_4/PVK vdW nanoheterojunction exhibits very good optical absorption characteristics in the visible-light wavelengths where g-C_3N_4 monolayer and PVK monomer act as electron donor and electron acceptor respectively. This character will facilitate the efficient separation and transportation of the photogenerated charges and thus increase the efficiency of the photocatalytic processes. These theoretical predictions provide insight to understand the related experimental observations, and verify that PVK monomer is a promising candidate as a non-noble metal co-catalyst for g-C_3N_4 photocatalysis.

Funding

This research received no external funding.

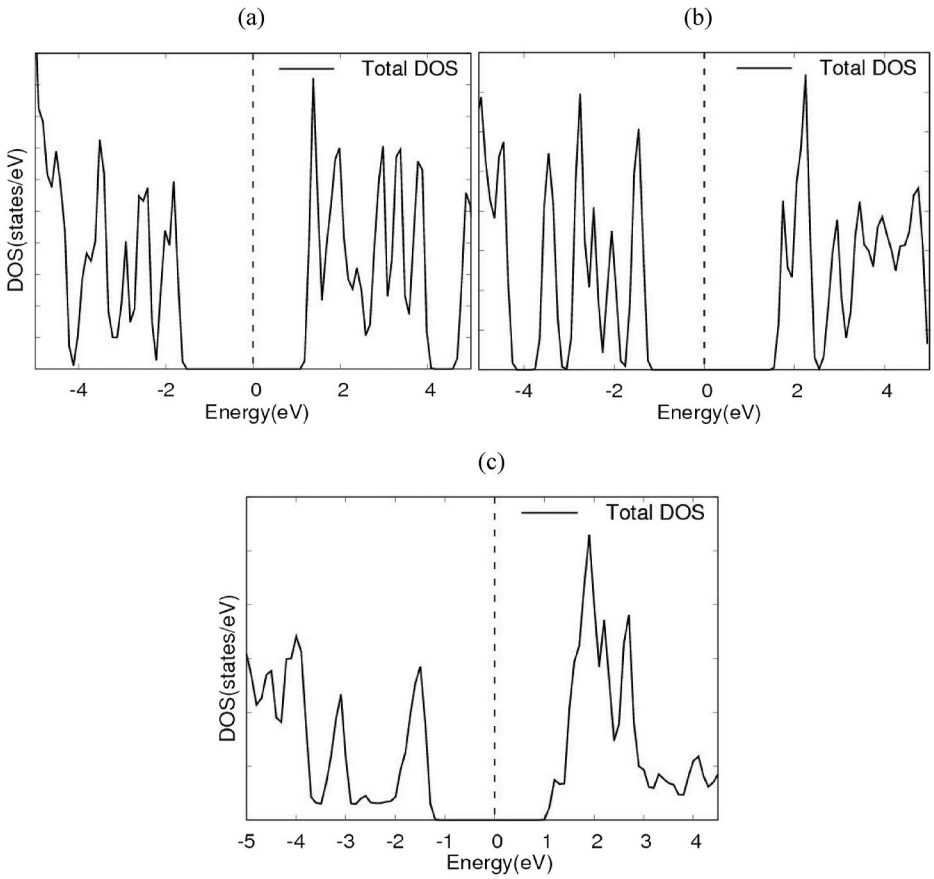

Fig. 6. Total electronic density of states (t-DOS) for (a) PVK, (b) monolayer g-C_3N_4 and (c) g-C_3N_4/PVK nanoheterojunction respectively. The Fermi energy level, E_F, is fixed as the reference of zero energy.

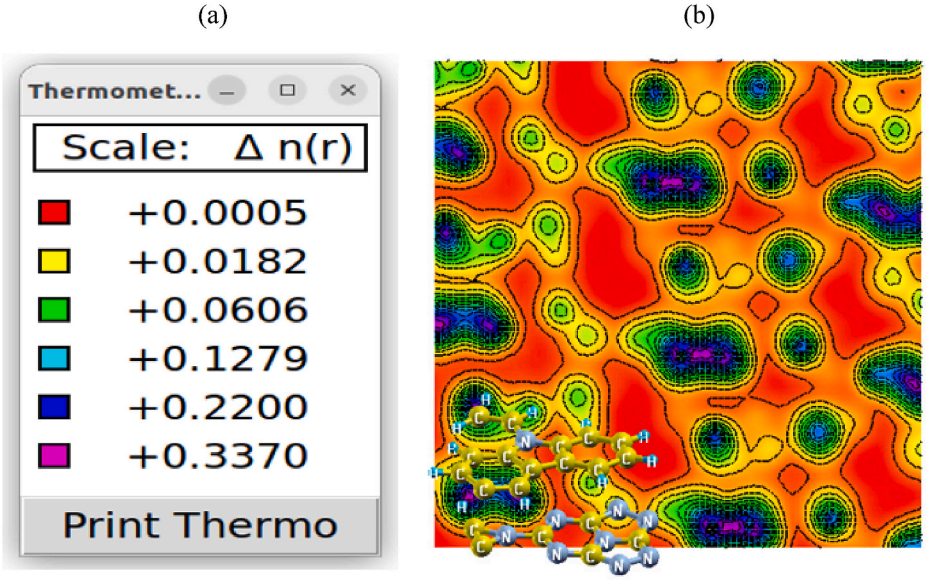

Fig. 7. Calculated self-consistent charge density isolines and isosurfaces of g-C_3N_4/PVK nanoheterojunction. The rainbow type color-coding refers to violet as regions of maximum charge density which decreases gradually finally to red as regions of minimum charge density. (For interpretation of the references to color in this figure legend, the reader is referred to the Web version of this article.)

CRediT authorship contribution statement

V.W. Elloh: Visualization, Investigation, Formal analysis, Writing – original draft. **E. Okoampa Boadu:** Visualization, Resources, Software, Data curation, repetition, Writing – review & editing. **D. Abbeyquaye:** Conceptualization, Data curation, Formal analysis, Funding acquisition, Writing – review & editing. **D.E. Anderson:** Methodology, Project administration, Resources, Software, Supervision, Validation. **A. Yaya:**

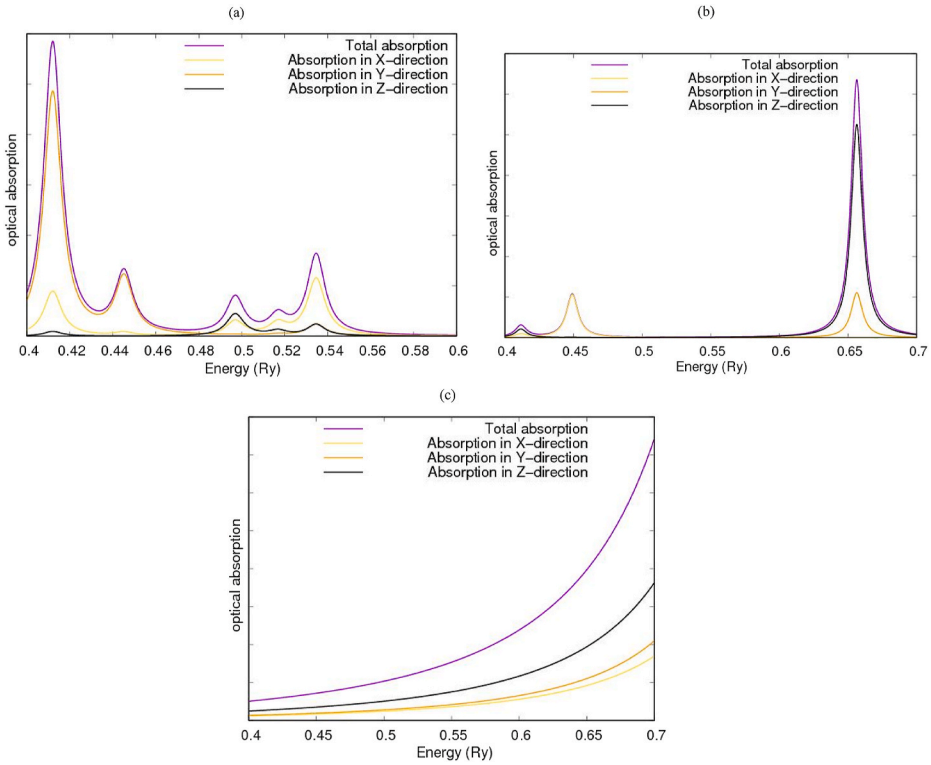

Fig. 8. Calculated (a) optical absorption spectra of PVK, (b) optical absorption spectra of monolayer g-C_3N_4 and (c) optical absorption spectra of g-C_3N_4/PVK nanoheterojunction respectively.

Supervision, Project administration, Funding acquisition, Visualization.

Declaration of competing interest

The authors declare that they have no known competing financial interests or personal relationships that could have appeared to influence the work reported in this paper.

Data availability

Data will be made available on request.

Acknowledgments

The authors would like to acknowledge the financial support from the Ghana Government Book and Research Allowance for tertiary institutions. V. W. E., acknowledges financial support from the University of Ghana Pan African Doctoral Academy. Authors are grateful to the Centre for High Performance Computing (CHPC), Cape Town, South Africa, for computer time on the Lengau cluster.

References

[1] S. Ye, R. Wang, M.Z. Wu, Y.P. Yuan, A review on g-C_3N_4 for photocatalytic water splitting and CO_2 reduction, Appl. Surf. Sci. 358 (2015) 15–27, https://doi.org/10.1016/j.apsusc.2015.08.173.

[2] W.J. Ong, L.L. Tan, Y.H. Ng, S.T. Yong, S.P. Chai, Graphitic carbon nitride (g-C_3N_4)-based photocatalysts for artificial photosynthesis and environmental remediation: are we a step closer to achieving sustainability? Chem. Rev. 116 (2016) 7159–7329, https://doi.org/10.1021/acs.chemrev.6b00075.

[3] J. Jiang, S. Cao, C. Hu, C. Chen, A comparison study of alkali metal-doped g- C_3N_4 for visible-light photocatalytic hydrogen evolution, Chin. J. Catal. 38 (2017) 1981–1989, https://doi.org/10.1016/s1872- 2067(17)62936-x.

[4] L. Liang, K. Li, K. Lv, W. Ho, Y. Duan, Highly photoreactive TiO_2 hollow microspheres with super thermal stability for acetone oxidation, Chin. J. Catal. 38 (2017) 2085–2093, https://doi.org/10.1016/s1872-2067(17)62952-8.

[5] S. Cao, J. Yu, Carbon-based H_2-production photocatalytic materials, J. Photochem. Photobiol., C 27 (2016) 72–99, https://doi.org/10.1016/j.jphotochemrev.2016.04.002.

[6] J. Low, B. Cheng, J. Yu, Surface modification and enhanced photocatalytic CO_2 reduction performance of TiO_2: a review, Appl. Surf. Sci. 392 (2017) 658–686, https://doi.org/10.1016/j.apsusc.2016.09.093.

[7] J. Lin, W. Tian, H. Zhang, X. Duan, H. Sun, S. Wang, Graphitic Carbon Nitride-Based Z-Scheme Structure for Photocatalytic CO_2 Reduction, Energy & Fuels, 2020, https://doi.org/10.1021/acs.energyfuels.0c03048.

[8] G. Zhang, G. Li, T. Heil, S. Zafeiratos, F. Lai, A. Savateev, M. Antonietti, X. Wang, Tailoring the grain boundary chemistry of polymeric carbon nitride for enhanced solar hydrogen production and CO_2 reduction, Angew. Chem. Int. Ed. 58 (2019) 3433–3437, https://doi.org/10.1002/anie.201811938.

[9] M.S. Akple, S.P. Chimmikuttanda, G.K.S. Takyi, V.W. Elloh, Fabrication and density functional theory calculations of bromine doped carbon nitride nanosheets with enhanced photocatalytic reduction of CO_2 into solar fuels, Jour. of Bioint. Rese. in Appl. Chem. 11 (2021) 14602–14619, https://doi.org/10.33263/BRIAC116.1460214619.

[10] S. Cao, J. Low, J. Yu, M. Jaroniec, Polymeric photocatalysts based on graphitic carbon nitride, Adv. Mater. 27 (2015) 2150–2176, https://doi.org/10.1002/adma.201500033.

[11] Y. Zhao, S. Xu, X. Sun, X. Xu, B. Gao, Unique bar-like sulfur-doped C_3N_4/TiO_2 nanocomposite: excellent visible light driven photocatalytic activity and mechanism study, Appl. Surf. Sci. 436 (2018) 873–881, https://doi.org/10.1016/j.apsusc.2017.12.061.

[12] H. Wang, L. Zhang, Z. Chen, J. Hu, S. Li, Z. Wang, J. Liu, X. Wang, Semiconductor heterojunction photocatalysts: design, construction and photocatalytic performances, Chem. Soc. Rev. 43 (2014) 5234–5244.

[13] A. Kubacka, M. Fernandez-Garcia, G. Colon, Advanced nanoarchitectures for solar photocatalytic applications, Chem. Rev. 112 (2012) 1555–1614.

[14] X. Wang, K. Maeda, A. Thomas, K. Takanabe, G. Xin, J. Carlsson, M. Domen, M. Antonietti, A metal-free polymeric photocatalyst for hydrogen production from water under visible light, Nat. Mater. 8 (2009) 76–80.

[15] J. Fu, K. Liu, K. Jiang, H. Li, P. An, W. Li, N. Zhang, H. Li, X. Xu, H. Zhou, Graphitic carbon nitride with dopant induced charge localization for enhanced photoreduction of CO_2 to CH_4, Adv. Sci. 6 (2019) 6, https://doi.org/10.1002/advs.201900796.

[16] L. Jiang, X. Yuan, Y. Pan, J. Liang, G. Zeng, Z. Wu, H. Wang, Doping of graphitic carbon nitride for photocatalysis: a reveiw, Appl. Catal., B 217 (2017) 388–406, https://doi.org/10.1016/j.apcatb.2017.06.003.

[17] S. Kumar, M.B. Gawande, J. Kopp, S. Kment, R.S. Varma, R. Zbořil, P-and F-co-doped carbon nitride nanocatalysts for photocatalytic CO_2 reduction and thermocatalytic furanics synthesis from sugars, ChemSusChem 13 (2020) 5231–5238, https://doi.org/10.1002/cssc.202001172.

[18] T. Mahvelati Shamsabadi, B.K. Lee, Photocatalytic H_2 evolution and CO_2 reduction over phosphorus-doped g-C_3N_4 nanostructures: electronic, Optical, and Surface properties, Renew. Sustain. Energy Rev. 130 (2020), https://doi.org/10.1016/j.rser.2020.109957.

[19] F. Xing, Q. Liu, M. Song, C. Huang, Fluorine modified boron carbon nitride semiconductors for improved photocatalytic CO_2 reduction under visible light, ChemCatChem 10 (2018) 5270–5279, https://doi.org/10.1002/cctc.201801418.

[20] J. Wang, S. Cao, J. Yu, Nanocages of polymeric carbon nitride from low-temperature supramolecular preorganization for photocatalytic CO_2 reduction, Solar RRL (2019), https://doi.org/10.1002/solr.201900469.

[21] M.S. Akple, T. Ishigaki, P. Madhusudan, Bio-inspired honeycomb-like graphitic carbon nitride for enhanced visible light photocatalytic CO_2 reduction activity, Environ. Sci. Pollut. Res. 27 (2020) 22604–22618, https://doi.org/10.1007/s11356-020-08804-2.

[22] S. Yin, J. Han, T. Zhou, R. Xu, Recent progress in g-C_3N_4 based low-cost photocatalytic system: activity enhancement and emerging applications, Catal. Sci. Technol. 5 (2015) 5048–5061, https://doi.org/10.1039/c5cy00938c.

[23] J. Liu, Y. Liu, N. Liu, Y. Han, X. Zhang, H. Huang, Y. Lifshitz, S.T. Lee, J. Zhong, Z. Kang, Metal-free efficient photocatalyst for stable visible water splitting via a two-electron pathway, Science 347 (2015) 970–974.

[24] Z. Li, J. Wang, K. Zhu, F. Ma, A. Meng, Ag/g-C_3N_4 composite nanosheets: synthesis and enhanced visible photocatalytic activities, Mater. Lett. 145 (2015) 167–170, https://doi.org/10.1016/j.matlet.2015.01.058.

[25] Q. Huang, J. Yu, S. Cao, C. Cui, B. Cheng, Efficient photocatalytic reduction of CO_2 by amine-functionalized g-C_3N_4, Appl. Surf. Sci. 358 (2015) 350–355, https://doi.org/10.1016/j.apsusc.2015.07.082.

[26] M.S. Akple, J. Low, S. Wageh, A.A. Al-Ghamdi, J. Yu, J. Zhang, Enhanced visible light photocatalytic H_2-production of g-C_3N_4/WS_2 composite heterostructures, Appl. Surf. Sci. 358 (2015) 196–203, https://doi.org/10.1016/j.apsusc.2015.08.250.

[27] H.J. Li, B.W. Sun, L. Sui, D.J. Qian, M. Chen, Preparation of water-dispersible porous g-C_3N_4 with improved photocatalytic activity by chemical oxidation, Phys. Chem. Chem. Phys. 17 (2015) 3309–3315, https://doi.org/10.1039/c4cp05020g.

[28] M. Shen, L. Zhang, J. Shi, Converting CO2 into fuels by graphitic carbon nitride-based photocatalysts, Nanotechnology 29 (2018) 29, https://doi.org/10.1088/1361-6528/aad4c8.

[29] Q. Liu, J. Shen, X. Yu, X. Yang, W. Liu, J. Yang, H. Tang, H. Xu, H. Li, Y. Li, Unveiling the origin of boosted photocatalytic hydrogen evolution in simultaneously (S, P, O)-Co-doped and exfoliated ultrathin g-C_3N_4 nanosheets, Appl. Catal., B 248 (2019) 84–94, https://doi.org/10.1016/j.apcatb.2019.02.020.

[30] Y. Zhou, W. Lv, B. Zhu, Tong, J. Pan, J. Bai, Q. Zhou, H. Qin, Template-free one-step synthesis of g-C_3N_4 nanosheets with simultaneous porous network and S-doping for remarkable visible-light-driven hydrogen evolution, ACS Sustain. Chem. Eng. 7 (2019) 5801–5807, https://doi.org/10.1021/acssuschemeng.8b05374.

[31] X. Song, X. Li, X. Zhang, Y. Wu, C. Ma, P. Huo, Y. Yan, Fabricating C and O co-doped carbon nitride with intramolecular donor-acceptor systems for efficient photoreduction of CO_2 to CO, Appl. Catal., B (2020) 268, https://doi.org/10.1016/j.apcatb.2020.118736.

[32] L. Jiang, X. Yuan, G. Zeng, J. Liang, Z. Wu, H. Yu, D. Mo, H. Wang, Z. Xiao, C. Zhou, Nitrogen self-doped g-C_3N_4 nanosheets with tunable band structures for enhanced photocatalytic tetracycline degradation, J. Colloid Interface Sci. 536 (2019) 17–29, https://doi.org/10.1016/j.jcis.2018.10.033.

[33] M.S. Akple, H.K. Apevienyeku, Synthesis and density-functional-theory calculations of electronic band structure of hollow sphere WS_2, Materials Science-Poland 36 (2018) 409–418, https://doi.org/10.2478/msp-2018-0052.

[34] B. Zhu, J. Zhang, C. Jiang, B. Cheng, J. Yu, First principles investigation of halogen-doped monolayer g-C_3N_4 photocatalyst, Appl. Catal., B 207 (2017) 27–34, https://doi.org/10.1016/j.apcatb.2017.02.020.

[35] S. Cao, J. Low, J. Yu, M. Jaroniec, Polymeric photocatalysts based on graphitic carbon nitride, Adv. Mater. 27 (2015) 2150–2176.

[36] S.J.A. Moniz, S.A. Shevlin, D.J. Martin, Z.X. Guo, J. Tang, Visible-light driven heterojunction photocatalysts for water splitting – a critical review, Energy Environ. Sci. 8 (2015) 731–759.

[37] Z. Zhao, Y. Sun, F. Dong, Graphitic carbon nitride-based nanocomposites: a review, Nanoscale 7 (2015) 15–37.

[38] C. Li, H. Wu, D. Zhu, T. Zhou, M. Yan, G. Chen, J. Sun, G. Dai, F. Ge, H. Dong, High-efficient charge separation driven directionally by pyridine rings grafted on carbon nitride edge for boosting photocatalytic hydrogen evolution, Appl. Catal. B Environ. 297 (2021), 120433, https://doi.org/10.1016/j.apcatb.2021.120433.

[39] C. Li, D. Zhu, S. Cheng, Y. Zuo, Y. Wang, C. Ma, H. Dong, Recent research progress of bimetallic phosphides-based nanomaterials as cocatalyst for photocatalytic hydrogen evolution, Chin. Chem. Lett. 33 (2022) 1141–1153, https://doi.org/10.1016/j.cclet.2021.07.057.

[40] C. Li, N. Su, H. Wu, C. Liu, G. Che, H. Dong, Synergies of adjacent sites in atomically dispersed ruthenium toward achieving stable hydrogen evolution, Inorg. Chem. 61 (34) (2022) 13453–13461, https://doi.org/10.1021/acs.inorgchem.2c01908.

[41] X.S. Rong, F.X. Qiu, H. Zhao, J. Yan, X.L. Zhu, D.Y. Yang, Fabrication of single-layer graphitic carbon nitride and coupled systems for the photocatalytic degradation of dyes under visible-light irradiation, Eur. J. Inorg. Chem. 2015 (2015) 1359–1367.

[42] M.L. Lu, Z.X. Pei, S.X. Weng, W.H. Feng, Z.B. Fang, Z.Y. Zheng, M.T. Huang, P. Liu, Constructing atomic layer g-C_3N_4-CdS nanoheterojunctions with efficiently enhanced visible light photocatalytic activity, Phys. Chem. Chem. Phys. 16 (2014) 21280–21288.

[43] P. Giannozzi, S. Baroni, N. Bonini, Quantum espresso: a modular and open-source software project for quantum simulations of materials, J. Phys. 21 (39) (2009), 395502. Article ID.

[44] J.P. Perdew, A. Zunger, Phys. Rev. B 23 (1981) 5048.

[45] J.P. Perdew, K. Burke, M. Ernzerhof, Phys. Rev. Lett. 77 (1996) 3865, 78 (1997) 1396.

[46] D. Vanderbilt, Soft self-consistent pseudopotentials in a generalized eigenvalue formalism. The Pseudopotential generation, Phys. Rev. B 41 (1990) 7892.

[47] S. Grimme, J. Antony, S. Ehrlich, H. Krieg, A consistent and accurate ab initio parametrization of density functional dispersion correction (Dft-D) for the 94 elements H-Pu, J. Chem. Phys. 132 (2010), 154104.

[48] H. Park, H.S. Koh, D.J. Siegel, First-Principles study of redox end members in lithium–sulfur batteries, J. Phys. Chem. C119 (2015) 4675–4683.

[49] Q. Guo, K.C. Lau, R. Pandey, A Xanes study of lithium polysulfide solids: a first-principles study, Mater. Adv. 2 (2021) 6403–6410.

[50] Q. Guo, K.C. Lau, R. Pandey, Thermodynamic and mechanical stability of crystalline phases of Li_2S_2, J. Phys. Chem. C123 (2019) 4674–4681.

[51] D.J. Hans, K. Ruth, Koordinatoren: Lexikon der Chemie In drei Bänden, vol. 3, Spektrum Verlag, Heidelberg, 1999, p. 92.

[52] Naoto Tsutsumi, Molecular design of photorefractive polymers, Polym. J. 48 (2016) 571–588.

[53] Y. Wang, N. Herron, J. Lumin, Poly(N-vinylcarbazole) (PVK) photoconductivity enhancement induced by doping with CdS nanocrystals through chemical hybridization, J. Phys. Chem. B70 (2000) 48.

[54] Microstructure evolution, thermal stability and fractal behavior of water vapor flow assisted in situ growth poly (vinylcarbazole)-titania quantum dots nanocomposites, D. Mombru, Jour. Phys. Chem. Solids 111 (2017) 199–206.

[55] R. Liu, Noncovalent functionalization of carbon nanotube using poly (vinylcarbazole)-based compatibilizer for reinforcement and conductivity improvement in epoxy composite, J. Appl. Polym. Sci. 134 (2017) 199–206.

[56] G.E. Hans, Poly(N-vinylcarbazol), in: Hans-Georg Elias: Makromoleküle Industrielle Polymere und Synthesen, vol. 3, Wiley-VCH, Weinheim, 2001, p. 211.

[57] X.L. Hu, Y.F. Zhang, N.F. Zhuang, J.Q. Qian, J. Solid State Chem. 183 (2010) 2741.

[58] T. Björkman, A. Gulans, A.V. Krasheninnikov, R.M. Nieminen, Van der Waals bonding in layered compounds from advanced density-functional first-principles calculations, Phys. Rev. Lett. 108 (2012) 235502–235507.

[59] H.L. Zhuang, R.G. Hennig, Single-layer group-III monochalcogenide photocatalysts for water splitting, Chem. Mater. 25 (2013) 3232–3238.

[60] J. Kang, S. Tongay, J. Zhou, J. Li, J. Wu, Band offsets and heterostructures of two-dimensional semiconductors, Appl. Phys. Lett. 102 (2013), 012111–012115.

[61] J. Liao, B. Sa, J. Zhou, R. Ahuja, Z. Sun, Design of high-efficiency visible-light photocatalysts for water splitting: MoS_2/AlN(GaN) heterostructures, J. Phys. Chem. C118 (2014) 17594–17599.

[62] A. Kokalj, Computer graphics and graphical user interfaces as tools in simulations of matter at the atomic scale, Comput. Mater. Sci. 28 (2003) 155–168.